CORA Cork Open Research Archive
Cartlann Taighde Oscailte Chorcaí

Title	Charge compensation and Ce3+ formation in trivalent doping of the CeO2(110) surface: The key role of dopant ionic radius
Authors	Nolan, Michael
Publication date	2011-03-10
Original Citation	Nolan, M. (2011) 'Charge compensation and Ce3+ formation in trivalent doping of the CeO2(110) surface: The key role of dopant ionic radius', Journal of Physical Chemistry C, 115(14), pp. 6671-6681. http://dx.doi.org/10.1021/jp112112u
Type of publication	Article (peer-reviewed)
Link to publisher's version	10.1021/jp112112u
Rights	© 2011 American Chemical Society. This document is the Accepted Manuscript version of a Published Work that appeared in final form in Journal of Physical Chemistry C, copyright © American Chemical Society after peer review and technical editing by the publisher. To access the final edited and published work see http://pubs.acs.org/doi/abs/10.1021/jp112112u
Download date	2026-11-06 06:22:34
Item downloaded from	https://hdl.handle.net/10468/2927

UCC
University College Cork, Ireland
Coláiste na hOllscoile Corcaigh

Charge Compensation and Ce^{3+} Formation in Trivalent Doping of the CeO_2 (110) surface: The Key Role of Dopant Ionic Radius

Michael Nolan

Tyndall National Institute, University College Cork, Lee Maltings, Prospect Row, Cork, Ireland

michael.nolan@tyndall.ie

RECEIVED DATE (to be automatically inserted after your manuscript is accepted if required according to the journal that you are submitting your paper to)

Running Head Title: Trivalent Doped Ceria

Abstract

In this paper we use density functional theory corrected for on-site Coulomb interactions (DFT+U) and hybrid DFT (HSE06 functional) to study the defects formed when the ceria (110) surface is doped with a series of trivalent dopants, namely Al^{3+}, Sc^{3+}, Y^{3+} and In^{3+}. Using the hybrid DFT HSE06 exchange correlation functional as a benchmark, we show that doping the (110) surface with a single trivalent ion leads to formation of a localised $M_{Ce}^{/}$ + $O_O^{\bullet}$ (M = the 3+ dopant), O^- hole state, confirming the description found with DFT+U. We use DFT+U to investigate the energetics of dopant compensation through formation of the $2M_{Ce}^{'}$ +$V_O^{\cdot\cdot}$ defect, i.e. compensation of two dopants with an oxygen vacancy. In conjunction with earlier work on La doped CeO_2, we find that the stability of the compensating anion vacancy depends on the dopant ionic radius. For Al^{3+}, which has the smallest ionic radius, and Sc^{3+} and In^{3+}, with intermediate ionic radii, formation of a compensating oxygen vacancy is stable. On the other hand, the Y^{3+} dopant, with an ionic radius close to that of Ce^{+4}, shows a positive anion vacancy formation energy, as does La^{3+}, which is larger than Ce^{4+} (*J. Phys. Cond. Matt.* **2010**, *20*, 135004). When considering the resulting electronic structure, in Al^{3+} doping, oxygen hole compensation is found. However, Sc^{3+}, In^{3+} and Y^{3+} show the formation of a reduced Ce^{3+} cation and an uncompensated oxygen hole, similar to La^{3+}. These results suggest that the ionic radius of trivalent dopants strongly influences the final defect formed when doping ceria with 3+ cations. In light of these findings, experimental investigations of these systems will be welcome.

Introduction

Cerium oxide (ceria) has been widely studied in catalysis for many years[1-5]. It has the ability to store and release oxygen, depending on the reaction conditions, a feature known as the oxygen storage capacity, OSC. Oxygen is released in a reducing atmosphere and taken up in an oxidising atmosphere. The OSC is facilitated by the ease with which Ce can change its oxidation state from 4+ in CeO_2 to 3+ in reduced ceria (with full reduction yielding Ce_2O_3) through formation of oxygen vacancies. This process results in transfer of two electrons from oxygen to Ce, with two Ce ions each being reduced to Ce^{3+}, giving partially reduced CeO_2. Partially reduced CeO_2 can be reoxidised by an oxygen source, e.g. the atmosphere or a molecule such as NO_2.

A large number of chemical reactions have been studied with ceria as catalyst, key amongst these being CO oxidation to CO_2[6-15]. This reaction follows the Mars van Krevelen mechanism[16], in which CO removes oxygen from the oxide. This oxygen is then replenished in some way, regenerating the catalyst. It is now understood that in order to enhance the formation of CO_2 from CO, the key quantity is the formation energy of an oxygen vacancy in the oxide – by making oxygen vacancy formation energy more favourable, the oxidation of CO can be enhanced. Recent work indicates that healing of the vacancy with gas phase oxygen[11,17] or with NO_2[18,19] is favourable so that the determining step is the initial removal of the oxygen vacancy. The formation energy of oxygen vacancy in bulk CeO_2 is *ca.*4.5 eV[20,22]. Calculations on the low index surfaces of ceria, namely (111), (110) and (100), show notably smaller oxygen vacancy formation energies[14,23-27].

However, recent experimental work has shown that the strategy of doping of ceria with other metal cations is one potentially fruitful means of enhancing CO oxidation[28-34]. This work has shown that metal dopants can enhance the oxygen vacancy formation energy and reactivity of ceria. In parallel, there have been a number of modelling studies of metal doping of ceria bulk and surfaces, which also show a smaller oxygen vacancy formation energy upon doping[11,12,34-44].

Trivalent dopants, such as La^{3+} and Eu^{3+}, have been investigated[28,32] and give an improved rate of conversion of CO to CO_2. However, this appears to happen only up to a certain concentration, of around

20% of the dopant. Beyond this concentration the reactivity decreases and this is thought to be due to separation into the individual oxides, CeO_2 and M_2O_3. In a previous study, we presented a first principles analysis of La^{3+} doping of the (111) and (110) ceria surfaces[43,45] and found the following: (i) La doping introduces a polaron hole state due to formation of localised O^-, (ii) formation of a compensating oxygen vacancy (which is the standard defect for lower valent doped systems) has an energy cost, (iii) when the oxygen vacancy forms the hole accompanying the dopant are not compensated, instead a Ce^{3+} ion and an oxygen hole are present and (iv) La doping of both surfaces makes them more reactive to CO oxidation compared to the undoped surfaces. This is particularly impressive for the (111) surface which when undoped shows no interaction with CO, a finding borne out by experimental work on CO oxidation[8,9] on ceria nanoparticles and reaction of oxygen with nanoparticles[46].

In that work, density functional theory corrected for on-site Coulomb interactions (DFT+U) was applied to Ce, which is a standard approach[47,48] that has been applied in many papers[10-12,14,17,18,20,23-26,35-45,49,50], but also to the O 2p states in order to correctly describe the oxygen hole that results upon trivalent doping of CeO_2[43,45]; the use of a +U correction on O 2p states stems from the need to describe localised oxygen polarons that result from substitutional doping of Ce with a lower valent dopant, as previously discussed for La doping of CeO_2. This approach has also been used to recover the oxygen polaron in other materials, such as Li-doped MgO[17,51], Al doped SiO_2[52] (see also refs. 53, 54); some further references on this general problem are[55-59]. As far as we are aware, La is the only trivalent dopant to have been modelled as a dopant in ceria using first principles simulations. With the unexpected behaviour of La doped CeO_2 it is therefore beneficial to investigate other trivalent dopants in CeO_2 in order to understand more generally the effect of aliovalent doping on the properties of ceria. While DFT+U is well established in studying ceria, it is not without problems, in particular the empiricism associated with a choice of U and the dependence of material properties on the value of U used in the calculation. Hybrid DFT in a plane wave basis set is now available and has been used in a number of papers over the last two years to study troublesome defect states in some metal oxides, including in ceria[26,41,42,60-62], providing an excellent description of many properties. Hybrid DFT is applied in form of

the screened exchange functional HSE06[63,64]. While hybrid DFT also includes parameters that need to be identified, namely the exchange contribution and the exchange screening distance, these have been determined to be most optimum at values of 25 % and 0.2 / Å [63,64] and are taken to be universal parameters. In addition, the cost of the hybrid DFT calculation in a plane wave basis set limits the size of the system that can be studied. For this paper, it is possible to study one trivalent dopant in the (110) surface with hybrid DFT.

This paper has two major aims; the first is to confirm the DFT+U description of trivalent doped CeO_2 using hybrid DFT and the second is to use DFT+U to study the charge compensation mechanism in trivalent doped CeO_2 and develop a more general understanding of doping in ceria. The dopants used are Al^{3+}, Sc^{3+}, In^{3+} and Y^{3+}, which have differing ionic radii – Al^{3+} being the smallest ion and Y^{3+} the largest ion. We also make reference to our previous results on La^{3+} doping where needed[43,45]. Comparison of the hybrid DFT and DFT+U results confirm the DFT+U description, so that for investigation of the anion vacancy compensation mechanism (which requires a larger surface supercell and a larger number of calculations), we can apply DFT+U.

Our results show that each dopant forms a localised oxygen hole on one or two oxygen atoms neighbouring the dopant. However the most stable defect, whether the oxygen hole polaron or the anion vacancy, depends on the ionic radius of the dopant. Al^{3+} is the smallest dopant and Y^{3+} is the closest in radius to Ce and the former results in oxygen vacancy compensation, while the latter is similar to La in that oxygen vacancy compensation is not spontaneous and results in a different electronic structure.

Methods

We use a slab model of the ceria (110) surface and a plane wave basis set to describe the valence electronic wave functions with the VASP code[65]. The cut-off for the kinetic energy is 396 eV. For the core-valence interaction we apply Blöchl's projector augmented wave (PAW) approach[66]. For Ce, we

use 12 valence electrons and for O a [He] core. For the dopants we use the following cores: Al^{3+} [Ne] core, Sc^{3+} [Ar] core, In^{3+} [Kr] core and Y^{3+} [Kr] core. Tables of ionic radii[67] show that Al^{3+}, Sc^{3+} and In^{3+} are smaller than Ce^{4+}, with Al^{3+} having a notably smaller ionic radius, while Y^{3+} has a larger ionic radius than Ce^{4+}. We use the Perdew-Burke-Ernzerhof (PBE) approximation for the exchange-correlation functional[68]. In common with other studies on ceria, we use density functional theory (DFT) corrected for on-site Coulomb interactions (DFT+U), where U^{Ce4f} = 5 eV and is applied to the Ce 4f states and, in addition, for oxygen, U^{O2p} = 7 eV and is applied to the O 2p states. The details of this approach and our choice of U are discussed extensively in refs. [23,24,43,45,51]. For some calculations, the hybrid HSE06 screened exchange functional is used, with a 25 % Hartree-Fock contribution and a screening length of 0.2 / Å. k-point sampling is performed using the Monkhorst-Pack scheme, with a (2x2x1) sampling grid.

In the Tasker classification[69], the (110) surface is a type I surface, with neutral CeO_2 planes along the slab. (2x2) and (4x2) surface cell expansions are used, in which one dopant gives an overall doping level of 1.8 % and 3.6 % for the larger and smaller surface cell expansions. In the (4x2) surface cell, two dopants gives a doping concentration of 3.6 %. The surface dopant concentration is 25 % in the smaller surface supercell and 12.5% in the larger surface supercell. The slab model for both surface expansions is 7 CeO_2 layers (11.5 Å) thick, with a 12 Å vacuum gap and the bottom two layers were fixed during the relaxations. All calculations are spin polarised with no restrictions on the overall spin.

It is well known that substituting an M^{4+} cation in a metal oxide with a lower valence M^{3+} cation results in formation of a localised electronic hole (a polaron) on an oxygen atom neighbouring the dopant[50-59]. This electronic hole gives rise to issues with the description of the resulting electronic structure using DFT, which we, for example, have discussed in detail for Li-doped MgO and Si-doped Al_2O_3[50-52] and in our previous work on La^{3+}-doping of ceria[43,45], providing a strong rationale for adopting this approach. Morgan and Watson[70] have also used U on oxygen in TiO_2 to describe localised states in defective TiO_2. Comparison of the DFT+U results will be made with the hybrid DFT for one dopant in the (2x2) surface cell.

The formation energy of an oxygen vacancy in doped ceria is given by

$E^{vac} = [E(M_{0.036}Ce_{1.964}O_{1.982}) + E(1/2O_2)] - E(M_{0.036}Ce_{1.964}O_2)$ (1)

with the dopant and vacancy concentrations calculated from the subscripts on the dopant, M, and O in (1). The energy of O_2 is computed using $U^{O2p} = 7$ eV for those calculations in which U^{O2p} is used on the oxide. Throughout this paper, a negative energy signifies that formation of an oxygen vacancy is favourable.

3. Results

3.1 A single trivalent dopant in the CeO_2 (110) surface

We begin by describing the atomic structure of the (110) surface with the introduction of one trivalent dopant. The undoped (110) surface has stoichiometric CeO_2 layers along the slab and the in surface layer the Ce-O distances are 2.34 Å and 2.32 Å to the first subsurface layer.

In figure 1, we show the top view of the (2x4) surface supercell with a dopant in the surface layer and we also show the pertinent dopant-O distances in Å. For Al^{3+} doping, the Al-O distances are 1.76 and 1.82 Å to surface oxygen and 1.78 and 1.81 Å to subsurface oxygen. There are two elongated Al-O distances, 3.09 and 3.26 Å – these are indicated with the dashed line between Al and O. The Ce-O distances in the surface are generally little changed, apart from those involving the oxygen atoms that move away from Al^{3+}. These oxygen have shorter distances to the nearest Ce ions and the local structure around the dopant is strongly distorted.

With Sc^{3+} doping, there is one elongated Sc-O distance of 2.46 Å, with the three remaining surface oxygens showing Sc-O distances of 2.31 (x2), and 2.05 Å. With In^{3+} doping, there is one elongated In-O distance of 2.36 Å, with three further In-O distances of 2.29 (x2) and 2.22 Å. Finally, with Y^{3+} doping, there is one Y-O distance of 2.46 Å and the remaining Y-O distances are 2.40, 2.31 and 2.29 Å. Thus, apart from Al doping, introduction of the dopant into the (110) ceria surface leads to formation of one elongated dopant-O distance in the surface. Al doping shows two elongated dopant-O distances.

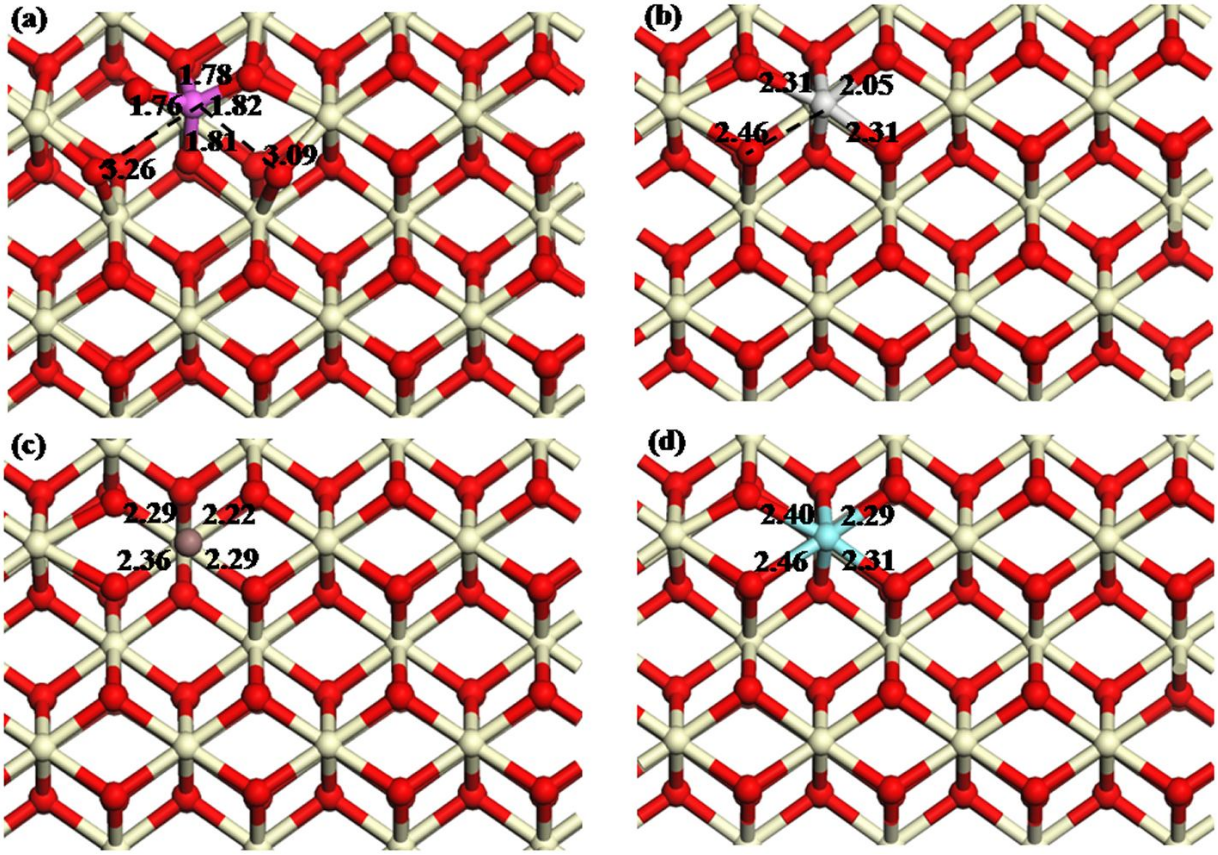


Figure 1: Structure around the dopant site for trivalent doped CeO_2 (110) surface from DFT+U using a (2x4) surface supercell. (a) Al^{3+}, (b) Sc^{3+}, (c) In^{3+} and (d) Y^{3+}. All distances are shown in Å.

It is interesting to consider the ionic radius of Ce and the dopants in understanding these distortions to the structures around the dopant. The ionic radius of Ce^{4+} is 0.87 Å, that of Al^{3+} is 0.39 Å, Sc^{3+} 0.75 Å, In^{3+} 0.80 Å and that of Y^{3+} 0.96 Å. Examining the dopant-O distances, we see that the very small Al^{3+} cation attempts to shorten as many cation-O distances as possible in order to obtain a coordination environment favourable for its ionic radius. This then leaves the remaining Al-O distances notably elongated, and results in a substantial distortion around the dopant site. As one goes from Sc^{3+} to In^{3+} to Y^{3+}, the dopant ionic radius approaches that of Ce^{4+} and the dopant is better able to be accommodated in the ceria lattice; the dopant-O distances and their more uniform distribution reflect the larger dopant ionic radii. For reference, La^{3+} has an ionic radius of 1.16 Å, and distorts the structure around its lattice site,

with longer La-O distances compared to the undoped surface; this arises from the larger size of La^{3+} relative to Ce^{4+}.

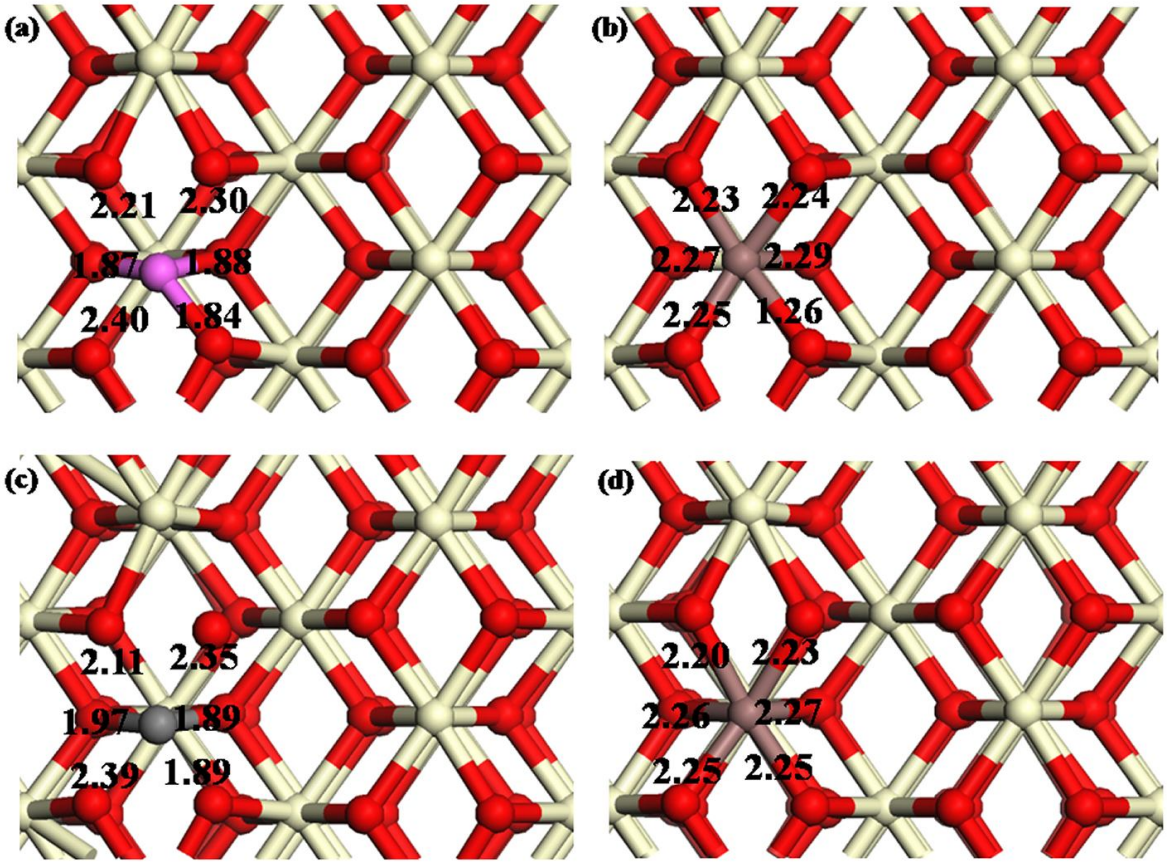


Figure 2 Structure around the dopant site for the example of Al^{3+} and In^{3+} doped CeO_2 (110) surface from (a) Al^{3+} DFT+U (b) In^{3+} DFT+U (c) Al^{3+} HSE06 (d) In3+HSE06 using a (2x2) surface supercell. All distances are shown in Å.

In figure 2 we show, for the example of Al^{3+} and In^{3+} as dopants, the DFT+U and HSE06 surface geometry of the doped (110) surface in a (2x2) surface supercell expansion. The shortened Al-O distances are 1.84, 1.87 1.88 and 2.21 Å, while the elongated Al-O distances are 2.39 and 2.40 Å with DFT+U. With HSE06, the same Al-O distances are 1.89, 1.89, 1.97 and 2.11 Å for the shorter Al-O distances and 2.35 and 2.39 Å for the longer Al-O distances.

For In^{3+}, the DFT+U In-O distances are 2.23, 2.24, 2.25, 2.26, 2.27 and 2.29 Å and with HSE06, the In-O distances are 2.20, 2.23, 2.25, 2.25, 2.26 and 2.27 Å. For Y doping, the Y-O distances with DFT+U are 2.20, 2.20, 2.30, 2.31, 2.36 and 2.44 A and with HSE06, they are 2.20, 2.21, 2.33, 2.33, 2.35 and 2.43 A. Thus, for larger dopants the difference between DFT+U and HSE atomic structure is quite small, as are the differences between the two surface supercells. For Al in the smaller surface supercell, while the DFT+U and hybrid DFT geometry around the dopant site are reasonably similar, there are quantitative differences that are more noticeable when compared with the larger dopants. Despite this, the geometry data give encouragement in using DFT+U to describe these systems.

Comparing, surface supercells, we do see a stronger distortion of the geometry around Al^{3+} in the larger surface supercell expansion. This may be a consequence of the effect of dopant concentration in each surface model, with the smaller surface supercell expansion putting more of a constraint on the extent of distortion possible upon doping. However, both models do show that Al^{3+} produces a large structural distortion upon substitution in the CeO_2 surface.

The spin densities for selected dopants in (a) the (2x2) surface supercell with DFT+U and HSE06 and (b) in the (2x4) surface supercell with DFT+U are shown in figure 3. In the larger surface supercell, Al^{3+} and Sc^{3+} doping results in formation of an oxygen hole that is predominantly localised on one oxygen atom, with a spin magnetisation of 0.75 (Al^{3+}) and 0.74 (Sc^{3+}) electrons and a spreading onto a second oxygen, which has a spin magnetisation of 0.15 electrons in both structures. For In^{3+}, the hole is split over two oxygen atoms, with spin magnetisation of 0.47 and 0.58 electrons (we were unable to find a stable solution with the hole localised on one oxygen atom). Finally, with Y^{3+}, the oxygen hole is localised onto one oxygen atom with a spin magnetisation of 0.75 electrons, while a second oxygen atom has a spin magnetisation of 0.15 electrons. With no +U correction on oxygen, we find the hole completely delocalised over the surface oxygen atoms of the (110) surface.

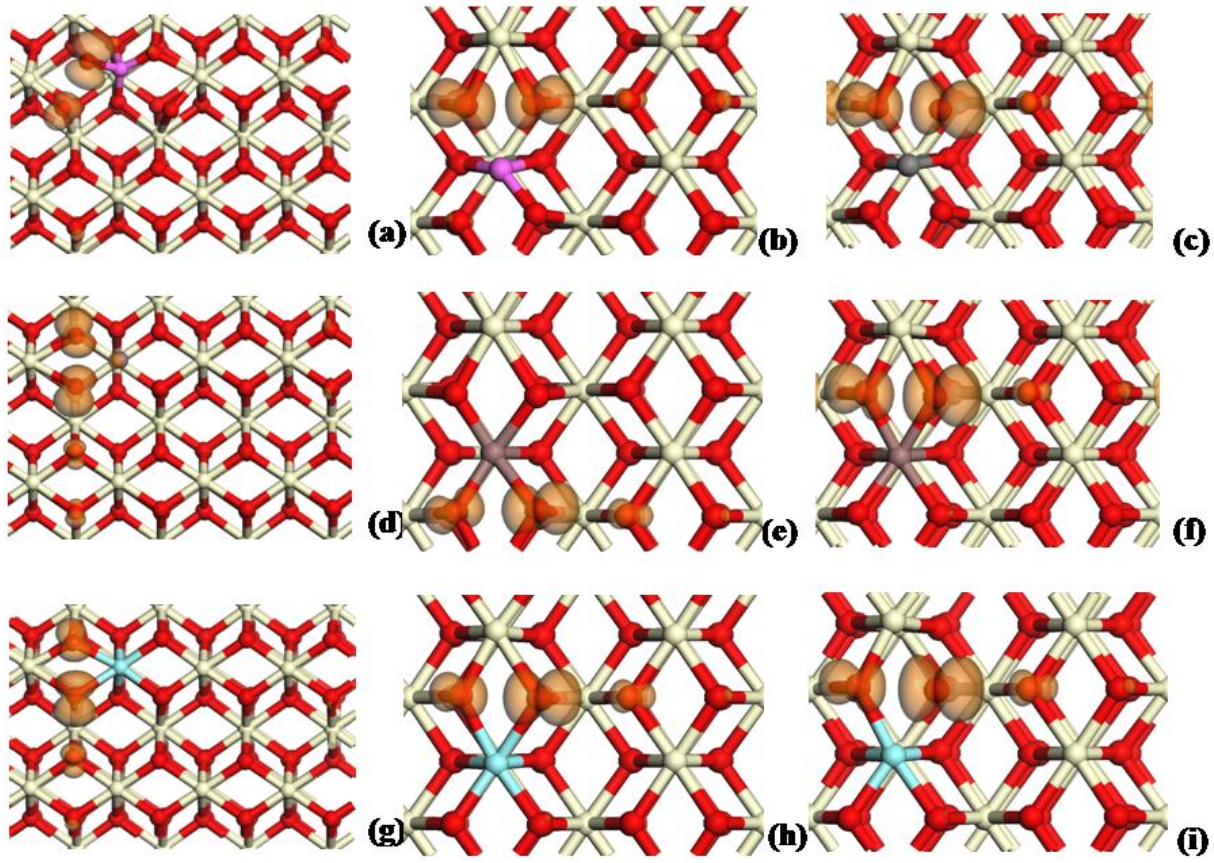


Figure 3: Spin density of selected trivalent doped CeO_2 (110) structures from DFT+U and hybrid DFT. (a) Al DFT+U (2x4) surface, (b) Al DFT+U (2x2) surface, (c) Al HSE (2x2) surface. (d) In DFT+U (2x4) surface, (e) In DFT+U (2x2) surface, (f) In HSE (2x2) surface. (g) Y DFT+U (2x4) surface, (h) Y DFT+U (2x2) surface, (i) Y HSE (2x2) surface.

Turning now to the smaller surface supercell, we compare the hole localisation with DFT+U and HSE06. For Al^{3+} doping, with both approaches the oxygen atom nearest Al^{3+} has a spin magnetisation of 0.40 (DFT+U) / 0.64 (HSE06) of the electron and the other oxygen has a spin density of 0.40 (DFT+U) / 0.22 (HSE06) of the electron; HSE06 gives stronger localisation onto a single oxygen neighbouring the dopant. With In^{3+} doping, the oxygen atom nearest In^{3+} has a spin magnetisation of 0.40 (DFT+U)/ 0.62 (HSE06) of the electron and the other oxygen having a spin density of 0.40 (DFT+U) / 0.27 (HSE06) of the electron. For Y^{3+}, on one oxygen has a spin magnetisation of 0.73 (DFT+U) / 0.70 (HSE06) electrons and a second oxygen atom has a spin magnetisation of 0.16 (DFT+U) / 0.15 (HSE06)

electrons. Thus, both DFT approaches give similar distributions of the oxygen polaron that results from trivalent doping, although Al^{3+} doping shows the largest differences between DFT+U and HSE06.

When comparing results between surface supercells, i.e. dopant concentration, it is interesting that the smaller doping concentration for the small ionic radius dopants leads to a less strong localisation of the oxygen hole with DFT+U. Hybrid DFT also shows this effect, but it is not as pronounced, so that there may be effects described by hybrid DFT that are not captured by the DFT+U approach.

The electronic density of states projected onto the Ce 4f and O 2p states of doped ceria (PEDOS) are plotted in figures 4 and 5 for the examples of Al^{3+} and Y^{3+} doping, respectively. The PEDOS for the other dopants is similar and is not shown. All dopants show a Ce 4f PEDOS typical for oxidised Ce^{4+}, with no states between the top of the valence band and the empty, narrow Ce 4f band. It is in the position of the gap state that the largest differences between the present DFT+U set-up and hybrid DFT are evident. The use of hybrid DFT results in a larger energy gap between the valence band and the unoccupied Ce 4f states (as well as between the valence band and the Ce 5d states); see also refs. 71,72. The energy gap with DFT+U depends on the value of U applied to the Ce 4f states and the O 2p states; the present values of U are chosen to describe consistently the formation of polaron states in reduced Ce and the O^{-} polaron. One could of course apply values of U that would recover the correct band gap of the host oxide, but these would then impact negatively on other material properties, e.g. for Ce, values of $U \geq 7eV$ position the Ce 4f states in the valence band. Thus, the choice of U parameters is always a compromise.

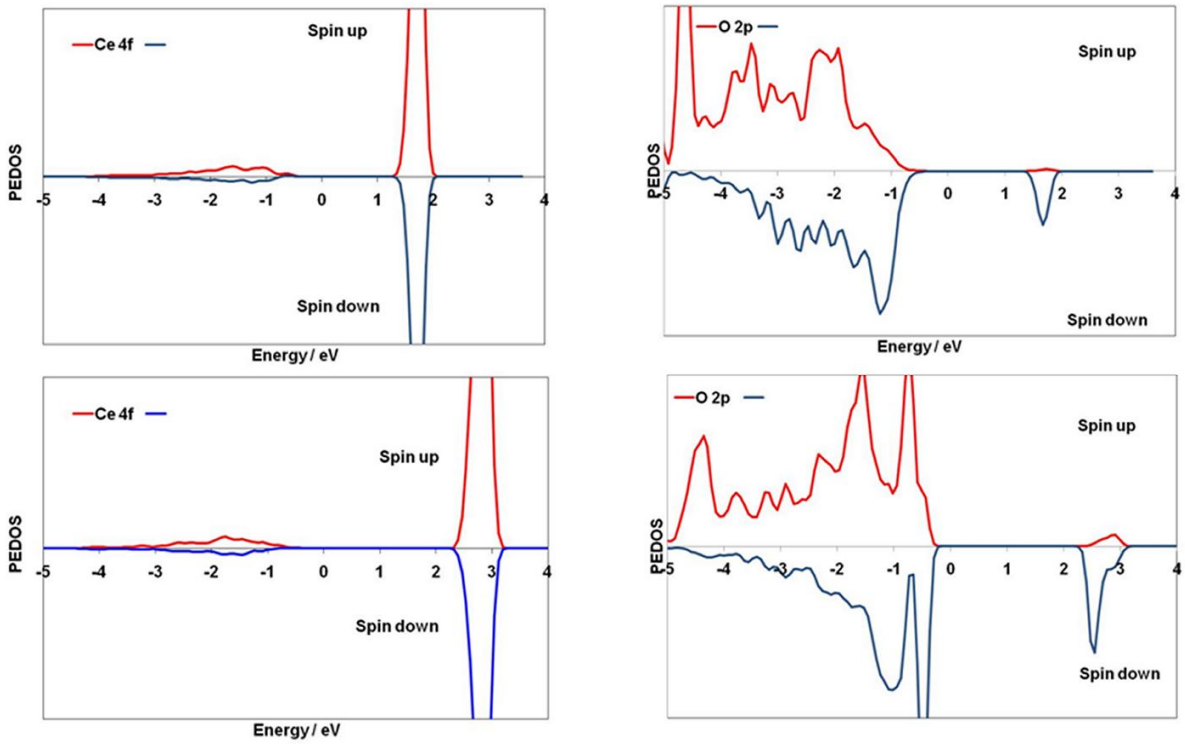


Figure 4: Ce and O 2p PEDOS for Al^{3+} doped CeO_2 (110) surface. Top panel: DFT+U, bottom panel: HSE06. The zero of energy in all plots is the Fermi level.

Turning to the oxygen 2p PEDOS, we see for both dopants that DFT+U and hybrid DFT result in formation of a spin down unoccupied state above the Fermi level (which is set to 0 eV in figures 4 and 5). This is the oxygen polaron state, arising from formation of a partially filled O 2p shell as a result of lower valent substitutional doping in ceria[43,45]. With DFT+U, this state lies 1.7 eV and 1.2 eV above the Fermi level for Al^{3+} and Y^{3+}, while with HSE06, the oxygen polaron state lies 2.5 eV and 2.1 eV above the Fermi level for Al and Y. The difference with HSE06 in terms of the position of the polaron electronic state is clear, with hybrid DFT giving a notably larger gap between the top of the valence band and the polaron state; a similar result is found for Sc^{3+} and In^{3+} doping (not shown). This difference has a simple origin in the energy gap between the valence band and conduction band found with DFT+U and hybrid DFT. The underestimation of this energy gap with DFT+U means that it is not possible to obtain the same position of the O^{-} polaron state with DFT+U as found with hybrid DFT. We have found the

same issue with trivalent dopants in rutile TiO_2 [72] and we make a general point that caution must be taken with the position of defect states in the band gap resulting from DFT+U calculations.

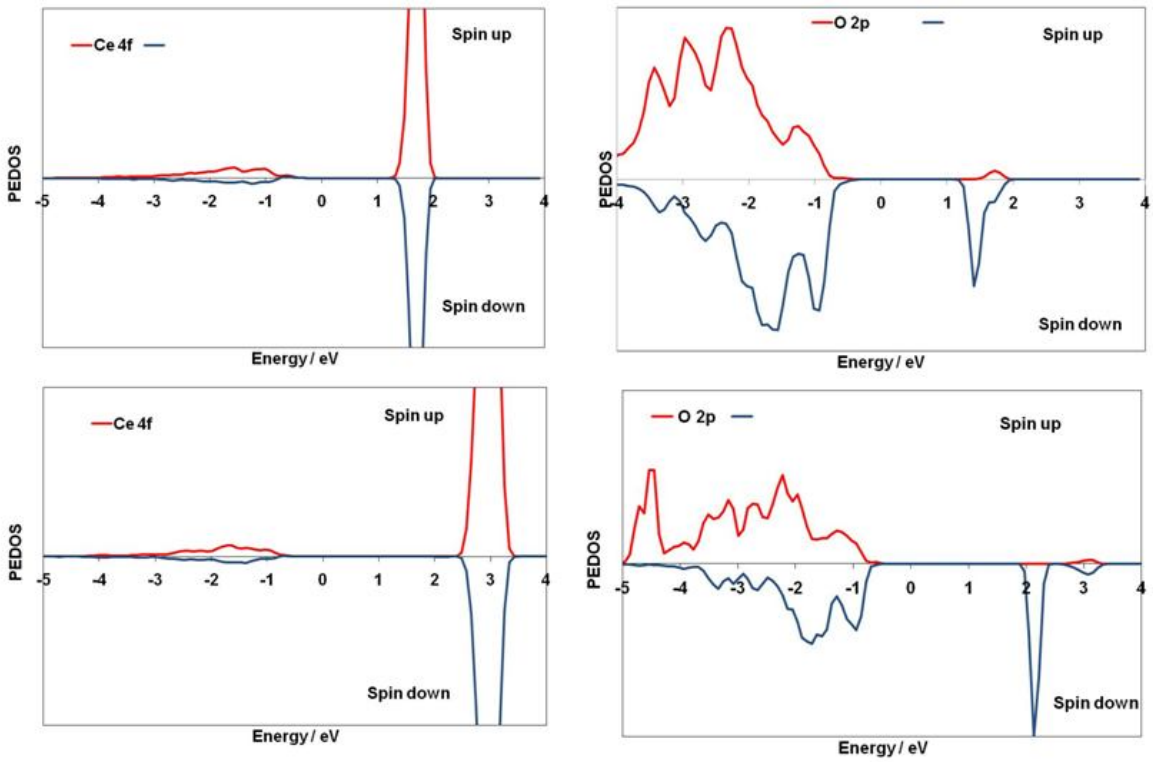


Figure 5: Ce and O 2p PEDOS for Y^{3+} doped CeO_2 (110) surface. Top panel: DFT+U, bottom panel: HSE06. The zero of energy in all plots is the Fermi level.

In general, while there are quantitative differences, the DFT+U and HSE06 descriptions of the formation of the oxygen hole polaron in trivalent doped CeO_2 are at least consistent, giving confidence in using DFT+U for subsequent calculations. In terms of dopant concentration, we do see some concentration effects when comparing the two different surface supercells, primarily that with a larger doping concentration for small ionic radius dopants, the distortions around the surface are less strong and the hole is apparently more equally shared between two oxygen atoms. Nonetheless, the essential features of the oxygen hole polaron are still captured in these calculations.

3.2 Formation of the Charge Compensating Oxygen Vacancy

We study charge compensating oxygen vacancies in the doped (2x4) surface supercell of the (110) surface to allow two dopants and an oxygen vacancy to be accommodated at reasonable concentrations; with 184 atoms, the size of this slab model means that hybrid DFT cannot be used here and all results from this point are with DFT+U. Figure 6 shows the atomic structure of the (110) surface with two dopants in their most stable substitutional sites. The geometries are similar to the case of a single dopant in the same surface supercell, as is the formation of the oxygen hole polaron.

In table 1 we show the oxygen vacancy formation energies for the most stable oxygen vacancy site in each oxygen vacancy compensated structure; the structures themselves are shown in figure 7. The formation energies of the compensating oxygen vacancy do not always fit with the generally assumed oxygen vacancy compensation model, in which a trivalent dopant is accompanied with spontaneous formation of a charge compensating oxygen vacancy, in contrast to refs. 72 and 73, where trivalent doping of TiO_2 is accompanied by formation of an oxygen vacancy. For Al^{3+}, Sc^{3+} and In^{3+}, since the computed formation energies are negative, this does indicate that spontaneous formation of a compensating oxygen vacancy can occur. However, for Y^{3+} and La^{3+} [43,45], the formation energies are positive so that charge compensation via oxygen vacancy formation is not necessarily spontaneous.

However, these are 0 K calculations and if one considers the effects of temperature and a real experimental environment, e.g. in water gas shift conditions, then formation of an oxygen vacancy will be more favourable, so that for each dopant one would expect formation of the compensating oxygen vacancy. Despite this, the trends found when comparing dopants should remain.

In addition, one must consider the possible errors in the DFT+U formation energies, which should be compared with hybrid DFT results – however, as discussed above, hybrid DFT simulations on the necessary structures are presently not feasible. Comparing with other oxides, we have shown that for trivalent doped TiO_2 [72], the formation energies of the charge compensating oxygen vacancy with hybrid

DFT are notably lower than the DFT+U formation energies, enhancing the stability of the oxygen vacancy compensated structures, although the qualitative trends in the energies were the same with both approaches. We have also found for divalent dopants in ceria (111) and (110) surfaces [74], that the hybrid DFT oxygen vacancy formation energies are lower (more negative) than the DFT+U formation energies. This leads us to suggest that for the present systems, a hybrid DFT calculation of the formation energy of the compensating oxygen vacancy will be more negative than the DFT+U formation energy, although the trends in stability with dopant ionic radius should be maintained.

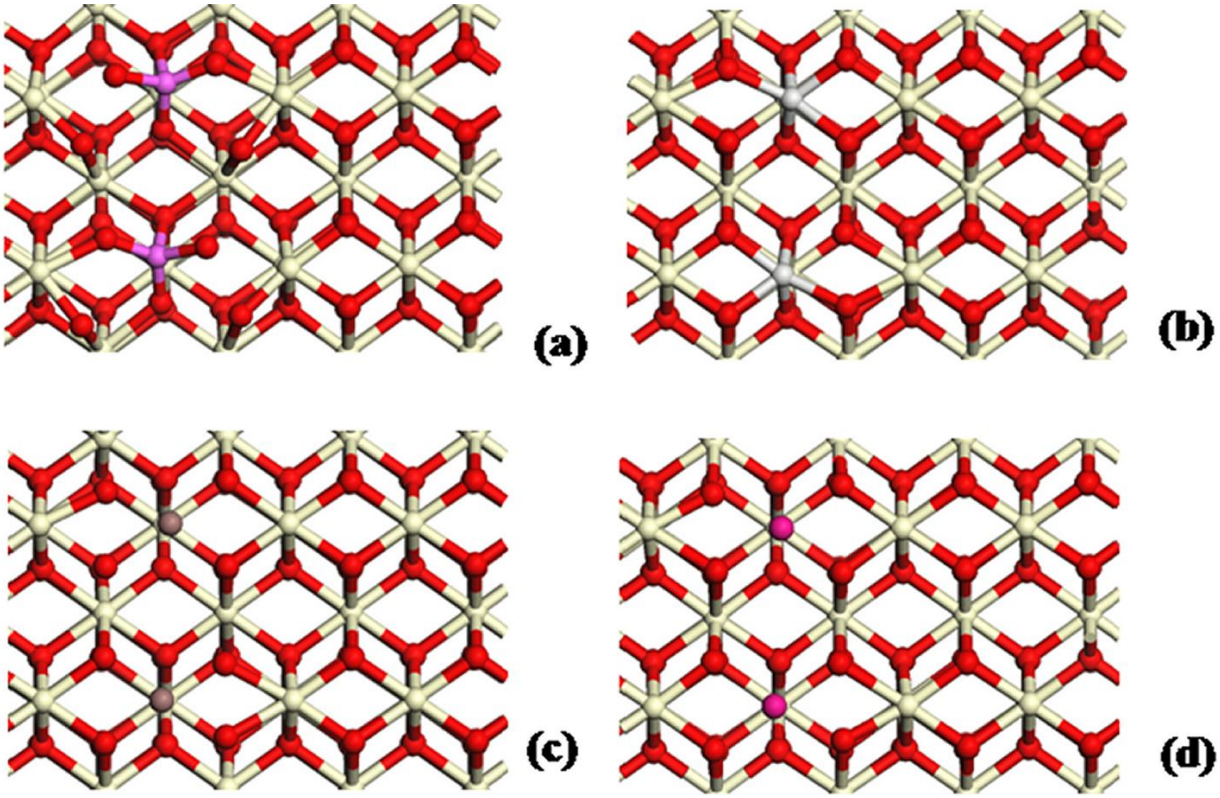


Figure 6: Atomic structure of the CeO_2 (110) surface in a (2x4) surface expansion with two substitutional dopants. (a) Al^{3+}, (b) Sc^{3+}, (c) In^{3+} and (d) Y^{3+}.

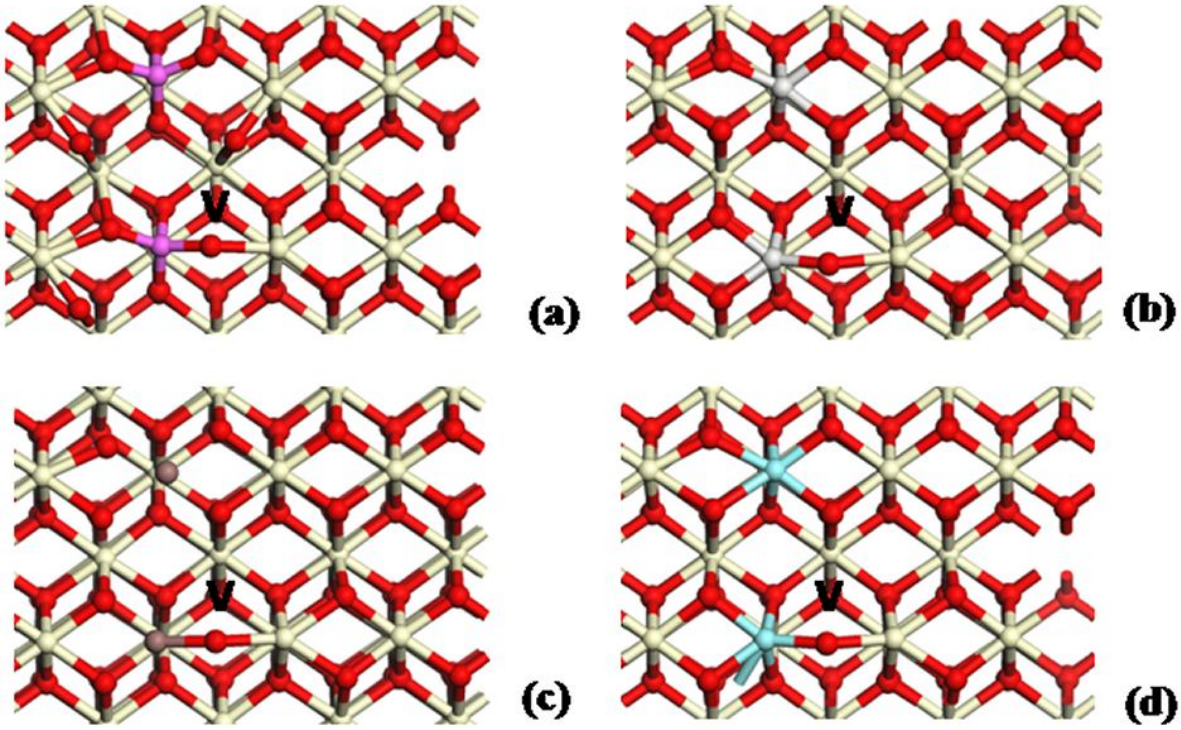


Fig. 7: Atomic structures of the most stable compensating oxygen vacancy sites in CeO_2 (110) surface. (a) Al^{3+}, (b) Sc^{3+}, (c) In^{3+} and (d) Y^{3+}. The vacancy site is indicated with a "V".

Dopant	Al	Sc	In	Y	La[a]
Dopant Ionic Radius / Å	0.39	0.75	0.80	0.96	1.16
$\mathbf{E^{Ovac}}$	-0.13	0.00	-0.18	+0.47	+0.65

Table **1:** Compensating oxygen vacancy formation energies, E^{Ovac}, for the dopants studied in this work in eV. A negative energy signifies that the oxygen vacancy will form spontaneously. The dopant ionic radii are given from ref. 75, with that of Ce^{4+} being 0.87 Å.

[a] the results for La^{3+} doping are from ref. 45 and are included for comparison

Taking these dopants together, there is a trend, as follows. The dopants with ionic radius smaller than Ce^{4+} have a preference to form the compensating oxygen vacancy, although the stabilisation of the oxygen vacancy structure is not large. The dopants with larger ionic radii than Ce^{4+} prefer not to form the oxygen vacancy compensated structure, showing an energy cost for formation of the oxygen vacancy, although this cost is not very high.

Let us now examine the electronic structure of the oxygen vacancy compensated structures, with the spin density in figure 8. It is expected that when the dopant is compensated with an oxygen vacancy, there will be no oxygen polaron states present. In figure 8(a) Al^{3+} shows compensation of the oxygen polaron as indicated by no spin density and the PEDOS in figure 9(a) shows no defect states.

For the other dopants, the situation is different. Figure 8(b)-(d) shows spin density plots for Sc^{3+}, In^{3+} and Y^{3+} doping with the compensating oxygen vacancy. In these plots we see spin density isosurfaces consistent with an oxygen hole polaron and reduced Ce^{3+}, which are confirmed by the PEDOS plots in figure 9 and the computed spin magnetisations. The PEDOS plots show states in the band gap due to the oxygen hole polaron and Ce^{3+}. The spin magnetisations on the Ce^{3+} ion are 0.95 (Sc^{3+}), 0.97 (In^{3+}) and 0.97 electrons (Y^{3+}) while the spin magnetisations on the polaron oxygen are 0.80 (Sc^{3+}), 0.74 (In^{3+}) and 0.72 electrons (Y^{3+}) We have also found this defect state to be the most stable for La doped (111) and (110) surfaces[43,45].

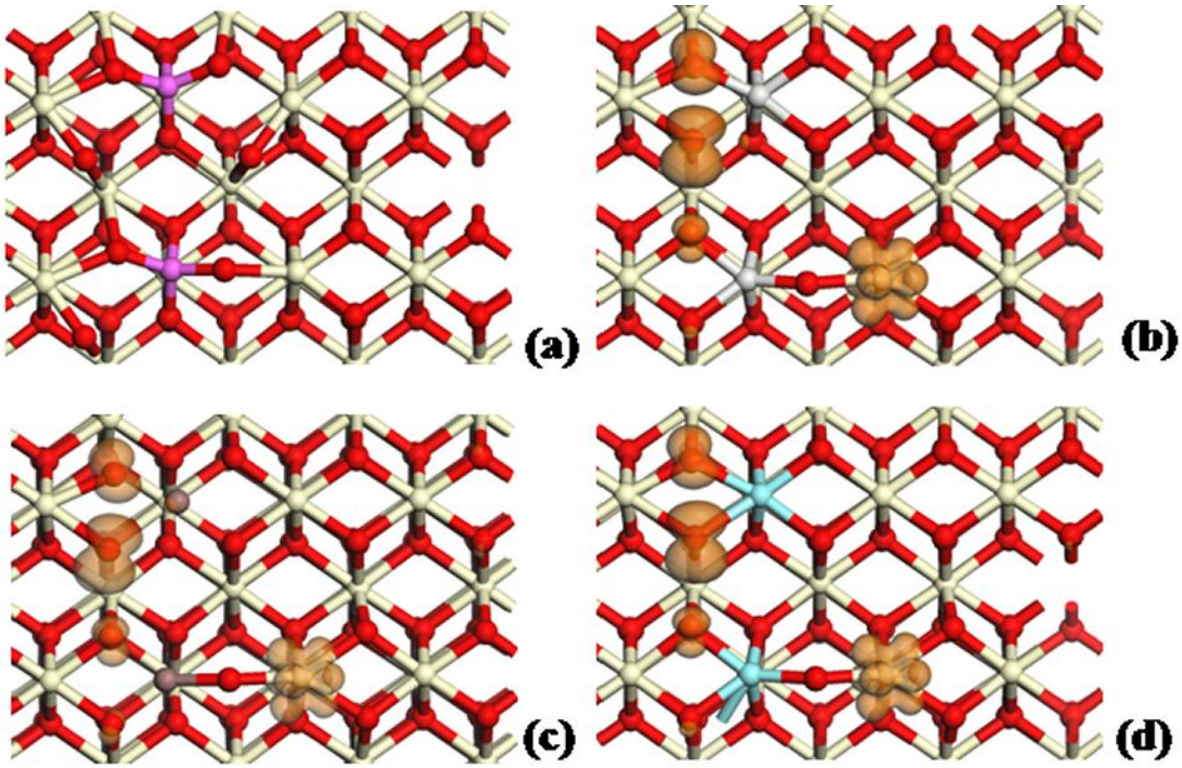


Figure 8: Spin density for two substituted 3+ dopants with a compensating oxygen vacancy. (a): Al^{3+}, (b) Sc^{3+}, (c) In^{3+} and (d) Y^{3+}.

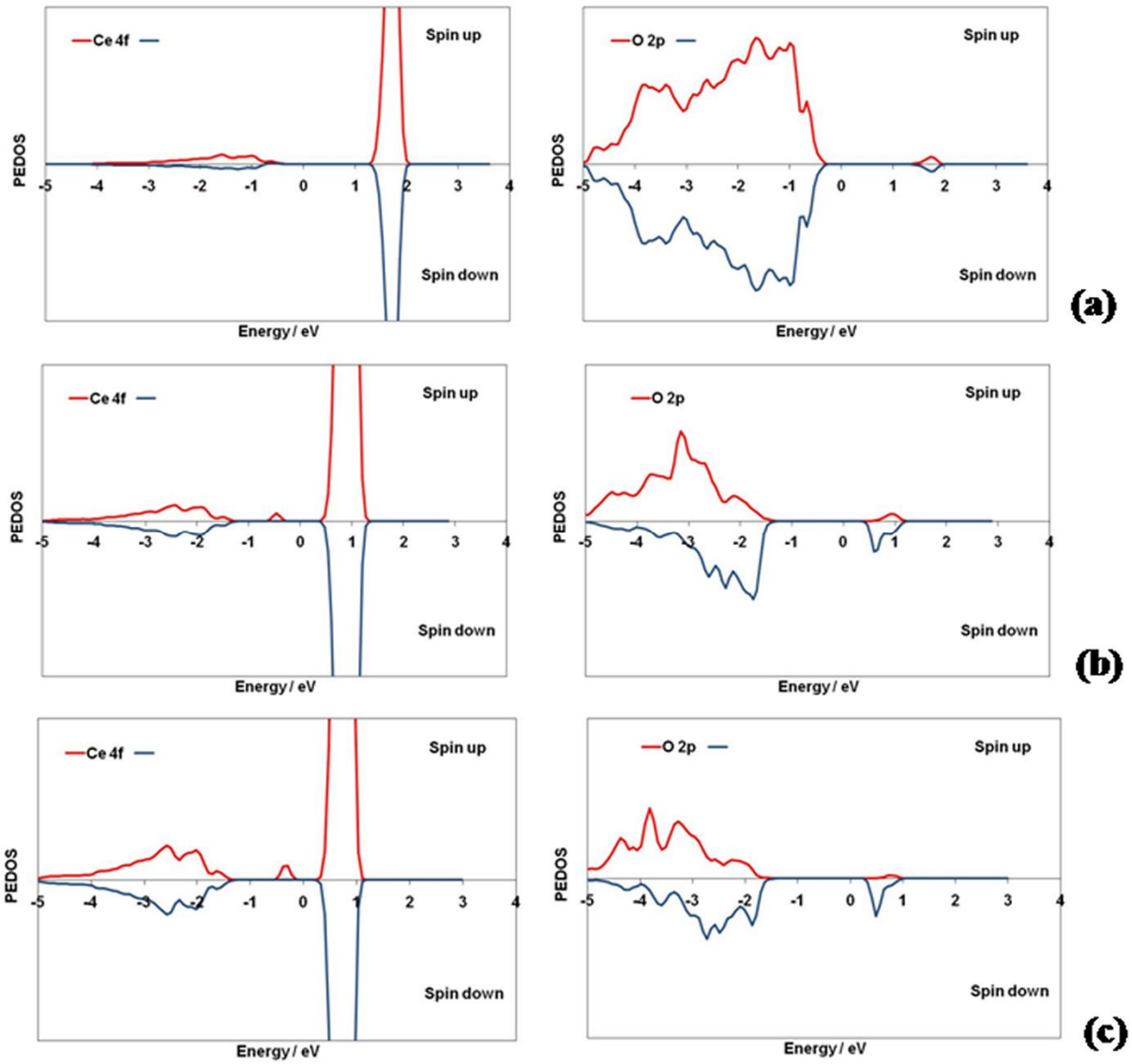


Figure 9: Ce 4f and O 2p PEDOS for two substituted 3+ dopants with a compensating oxygen vacancy. (a) Al^{3+}, (b) In^{3+}, (c) Y^{3+}. The zero of energy is the Fermi level.

It may be surprising that oxygen vacancy compensation on some trivalent doped ceria surfaces results in formation of Ce^{3+} and an oxygen hole, since it is generally accepted that the formation of an oxygen vacancy defect compensates an aliovalent dopant with a lower oxidation state; for example, in Li-doped MgO (even with U = 7 eV on O 2p states), oxygen vacancy formation always compensates the two electronic holes[17]. For TiO_2 it is known that an Al dopant is compensated with an oxygen vacancy[59,72,73].

A well known example is trivalent doped zirconia in refs 76 and 77, where oxygen vacancies are found to compensate the oxygen hole introduced by the dopant. In these examples, we see that hole compensation is favoured over cation reduction, since Mg and Zr are not reducible, although TiO_2 is considered a reducible oxide.

In our previous work[43,45], we suggested that the results for La doped CeO_2 can be best understood by considering the nature of the host oxide: Cerium is more easily reduced compared to the cations above, and formation of an oxygen vacancy resulting in formation of reduced Ce^{3+} is quite favourable. In general, we propose that energetics of cerium reduction mean that upon oxygen vacancy formation, it is favourable to reduce one Ce^{4+} ion to Ce^{3+} and compensate one oxygen hole, rather than compensate both electronic holes as in other oxides, so that a key role in determining the defects formed upon trivalent doping of ceria is played by the cerium cation. In contrast, TiO_2 shows only compensation of the oxygen hole upon oxygen vacancy formation.

However, Al^{3+} as a trivalent dopant in CeO_2 appears to be an exception, in that its defect chemistry leads to spontaneous compensation of the oxygen holes. We attribute this to the smaller ionic radius of Al^{3+} compared with Ce^{4+} (and the other cation dopants considered), which leads to the strongest distortions around the dopant site. It is most likely that these distortions favour the compensation of the oxygen hole over formation of Ce^{3+}. This finding highlights the complexity in determining the impact of dopant on the stable defect state in doped ceria. It is not simply enough to consider the different oxidation states of the dopant and the host cation. One must also consider local coordination environment and dopant ionic radius and examine the effect of the dopant on the defects that are formed. In any case, experimental investigations of these systems to establish their stable defects are suggested.

Conclusions

When the (110) surface of ceria is doped with trivalent cations, the most stable defect depends on the ionic radius of the dopant. For small ionic radius dopants, with a large mismatch to the host oxide, the structure is strongly distorted. For Al, Sc and In, we the most stable defect is the oxygen vacancy

compensating two dopants. For Y and La, the most stable defect is $M_{Ce}^{/} + O_O^{\bullet}$ with one dopant and an oxygen hole. It is also very interesting that for Al, the electronic structure is typical of the classical oxygen vacancy compensating defect mechanism, but in this structure, the other dopants all show formation of a reduced Ce^{3+} ion and an uncompensated oxygen hole. We attribute this to the ease of reducibility of Ce and urge experiments on these systems to establish the nature of the defect in trivalent doped ceria.

Acknowledgements

We acknowledge support from Science Foundation Ireland through the Starting Investigator Research Grant Program (EMOIN (SIRG/09/I1620)). We acknowledge a grant of computer time at Tyndall from Science Foundation Ireland, and the SFI/Higher Education Authority funded Irish Centre for High End Computing (ICHEC) for the provision of computational facilities. We thank Prof. M. A. Morris and Dr. P. Fleming for valuable discussions.

References

1. Trovarelli, A. Catalysis by Ceria and Related Materials, Imperial College Press, UK, 2002.

2. Trovarelli, A. *Catalysis Reviews – Science and Engineering* **1996,** *38*, 439

3. Gorte, R. J., *AiChE Journal,* **2010,** *56,* 1126

4. Han, W-Q.; Wen, W.; Hanson, J. C.; Teng, X.; Marinkovic, N.; Rodriguez, J. A. *J. Phys. Chem. C* **2009,** *113,* 21949

5. Vivier, L.; Duprez, D. *ChemSusChem* **2010,** *3,* 654

6 Li, C.; Sakata, Y.; Arai, T.; Domen, K.; Maruya, K.; Onishi, T. *J. Chem. Soc. Faraday Trans. 1* **1989,** *85,* 929

7. Li, C.; Sakata, Y.; Arai, T.; Domen, K.; Maruya, K.; Onishi, T. *J. Chem. Soc. Faraday Trans. 1* **1989,** *85,* 1451

8 Aneggi, E.; Llorca, J.; Boaro, M.; Trovarelli, A. *J. Catal.* **2005,** *234,* 88

9 Zhou, K. B.; Wang, X.; Sun, X.M.; Peng, Q.; Li, Y. D. *Journal of Catalysis* **2005,** *229*, 206

10 Nolan, M.; Watson, G. W. *J. Phys. Chem. B* **2006, 110B**, 16600

11 Shapovalov, V.; Metiu, H. *J. Cat.* **2007,** *245,* 205

12 Nolan, M.; Soto-Verdugo, V.; Metiu, H. *Surf Sci.* **2008**, *602*, 2734

13. Manzoli, M.; Boccuzzi, F.; Chiorino, A.; Vindigni, F.; Deng, W.; Flytzani-Stephanopoulos, M. *Journal of Catalysis* **2007**, *245*, 308

14 Scanlon, D. O.; Walsh, A.; Morgan, B. J.; Nolan, M.; Fearon, J.; Watson, G. W. *J. Phys. Chem C.* **2007,** *111*, 7971

15 Huang, M.; Fabris, S. *J. Phys. Chem. C* **2008,** *112*, 8643

16 Mars, P.; van Krevelen, D. W.. *Chem. Eng. Sci. Spec. Suppl.* **1954,** *3,* 41

17 Nolan, M. *J. Chem. Phys.,* **2009**, *131*, 144702

18 Nolan, M.; Parker, S. C.; Watson, G. W. *J. Phys. Chem. B,* **2006**, *110*, 2256

19 Namai, Y.; Fukui, K.; Iwasawa, Y. *Nanotechnology* **2004**, *15*, S49

20 Nolan, M.; Fearon, J. E.; Watson, G. W. *Solid State Ionics* **2006**, *177*, 306

21 Keating, P. R. L.; Scanlon, D. O.; Watson, G. W. *J. Phys. Condens. Matt.,* **2009**, *21*, 405502

22 Fabris, S.; de Gironcoli, S.; Baroni, S.; Vicario, G.; Balducci, G. *Phys. Rev. B* **2005,** *71,* 041102

23. Nolan, M.; Grigoleit, S.; Sayle, D. C.; Parker, S. C.; Watson, G. W. *Surf. Sci.* **2005,** *576*, 217

24. Nolan, M.; Parker, S. C.; Watson, G. W. *Surf. Sci.* **2005,** *595*, 223

25. Fabris, S.; Vicario, G.; Balducci, G.; de Gironcoli, S.; Baroni, S. *J. Phys. Chem. B* **2005,** *109*, 22860

26. Ganduglia-Pirovano, M. V.; Da Silva, J. L. F.; Sauer, J. *Phys. Rev. Lett.,* **2009,** *102*, 026101

27. Sayle

28. Patl, S.; Seal, S.; Guo, Y.; Schulte, A.; Norwood, J. *Appl. Phys. Lett.,* **2006,** *88*, 243110

29. Ou, D. R.; Mori, T.; Ye, F.; Kobayashi, T.; Zuo, J.; Auchterlonie, G.; Drennan, J. *Appl. Phys. Lett.,* **2006,** *89*, 171911

30. Dutta, G.; Waghmare, U. V.; Baidya, T.; Hegde, M. S.; Priolkar, K. R.; Sarode, P. R. *Cat. Lett.* **2006,** *108*, 165

31. Dutta, G.; Waghmare, U. V.; Baidya, T.; Hegde, M. S.; Priolkar, K. R.; Sarode, P. R. *Chem. Mat.* **2006,** *18*, 3249

32. Hernandez, W. Y.; Centeno, M. A.; Romero-Sarria, F.; Odriozola, J. A. *J. Phys. Chem. C* **2009,** *113*, 5629

33. Kadowaki, H.; Saito, N.; Nishiyama, H.; Inoue, Y. *Chem. Lett*. **2007,** *36*, 440

34. Tang, W.; Hu, Z.; Wang, M.; Stucky, G. D.; Metiu, H.; McFarland, E. W., *J. Catalysis* **2010,** *273*, 125

35. Andersson, D. A.; Simak, S. I.; Skorodumova, N. V.; Abrikosov, I. A.; Johansson, B. *Appl. Phys. Lett.* **2007,** *90,* 031909

36. Yang, Z.; Luo, G.; Lu, Z. Hermansson, K. *J. Chem. Phys.* **2007,** *127*, 074704

37. Yang, Z.; Lu, Z.; Luo, G. *Phys. Rev. B* **2007,** *76,* 075421

38. Wang, X. Q.; Rodriguez, J. A.; Hanson, J. C.; Gamara, D.; Martinez-Arias, A.; Fernandez-Garcia, M. *J. Phys Chem. B* **2005,** *109*, 19595

39. Balducci, G.; Islam, M. S.; Kaspar, J.; Fornasiero, P.; Graziani, M.; *Chem. Mat.* **2000,** *12*, 677

40. Wang, H-F.; Gong, X-Q.; Guo, Y-L.; Guo, Y.; Lu, G. Z.; Hu, P. *J. Phys. Chem C* **2009,** *113*, 10229

41 Nolan, M. *J. Phys. Chem. C,* **2009**, *113*, 2425

42. Nolan, M. *Chem. Phys. Lett.,* **2010**, *492*, 115

43. Yeriskin, I.; Nolan, M. *J. Chem. Phys.,* **2009**, *131*, 244702

44. Yang, Z.; Wei, W.; Fu, Z.; Lu, Z.; Hermansson, K. *Surf. Sci.,* **2008**, *602*, 1199

45. Yeriskin, I.; Nolan, M. *J. Phys. Cond. Matt.* **2010,** *22, 135004*

46. Wu, Z.; Li, M.; Howe, J.; Meyer III, H. M.; Overbury, S. H. *Langmuir*, **2010**, *26* 16595

47. Anisimov, V. I.; Zaanen, J.; Andersen, O. K.; *Phys. Rev B* **1991,** *44,* 943

48. Dudarev, S. L.; Botton, G. A.; Savrasov, S. Y.; Humphreys, C. J.; Sutton, A. P.; *Phys. Rev. B* **1998,** *57*, 1505

49. Castleton, C. W. M.; Kullgren, J.; Hermansson, K. *J. Chem. Phys.,* **2007,** *127*, 244704

50. Ganduglia-Pirovano, M. V.; Hofmann, A.; Sauer J. *Surf Sci. Rep.*, **2007***, 62,* 219

51. Nolan, M.; Watson, G. W. *Surf. Sci.* **2005,** *586*, 25

52. Nolan, M.; Watson, G. W. *J. Chem. Phys.* **2006,** *125*, 144701

53. Laegsgaard, J.; Stokbro, K. *Phys. Rev. B* **2002,** *65*, 075208

54. Pacchioni, G.; Frigoli, F.; Ricci, D.; Weil, J. A. *Phys. Rev. B* **2001,** *63*, 054102

55. Schirmer, O. F. *J. Phys. Cond. Matt.* **2006,** *18,* R667

56. Stoneham, A. M.; Gavartin, J.; Shluger, A. L.; Kimmel, A. V.; Munoz Ramos, D.; Ronnow, H. M.; Aeppli, G.; Renner, C. *J. Phys. Cond. Matt.* **2007,** *19*, 255208

57. Du, M. H.; Zhang, S. B. *Phys. Rev. B* **2009,** *80*, 115217

58. Stashans, A.; Bermeo, S. *Chem. Phys.* **2009,** *363*, 100

59. Islam, M. M.; Bredow, T.; Gerson, A. *Phys. Rev. B* **2007,** *76*, 045217

60. Da Silva, J. L. F.; Ganduglia-Pirovano, M. V.; Sauer, J.; Bayer, V.; Kresse, G. *Phys. Rev. B*, **2007**, *75*, 045121

61. Scanlon, D. O.; Morgan, B. J.; Watson, G. W.; Walsh, A. *Phys Rev. Lett,* **2009**, *103*, 096405

62. Ágoston, P.; Albe, K.; Nieminen, R. M.; Puska, M. J. *Phys. Rev. Lett.* **2009, *103***, 245501

63 Janesko, B. G.; Henderson, T. M.; Scuseria, G. E. *Phys. Chem. Chem. Phys.* **2009,** *11*, 443

64 Henderson, T. M.; Paier, J.; Scuseria, G. E. *Phys. Stat. Sol. B* **2010** doi:10.1002/pssb.201046303

65. Kresse, G.; Hafner, J. *Phys. Rev. B* **2004,** *49*, 14251; Kresse, G.; Furthmüller, J. *Comp. Mat. Sci* **1996,** *6*, 5

66. Blöchl, P. E.; *Phys. Rev. B* **1994,** *50,* 17953; Joubert, D.; Kresse, G. *Phys. Rev. B* **1999,** *59*, 1758

67. Shannon, R. D. *Acta Cryst.* **1976,** *A32,* 751

68. Perdew, J. P.; Burke, K.; Ernzerhof, M. *Phys. Rev. Lett.***1996,** *77,* 3865

69. Tasker, P. W. *J. Phys. C* **1980,** *6,* 488

70. Morgan, B. J.; Watson, G. W. *J. Phys. Chem. C,* **2009**, *113*, 7322

71. Nolan, M. *Chem. Phys. Lett.,* **2010,** *499,* 126

72. Iwaszuk, A.; Nolan, M. *J. Phys. Condens. Matt.,* **2011,** *in press*

73. Gesenhues, U. *Journal of Photochemistry and Photobiology A* **2001,** *139*, 243

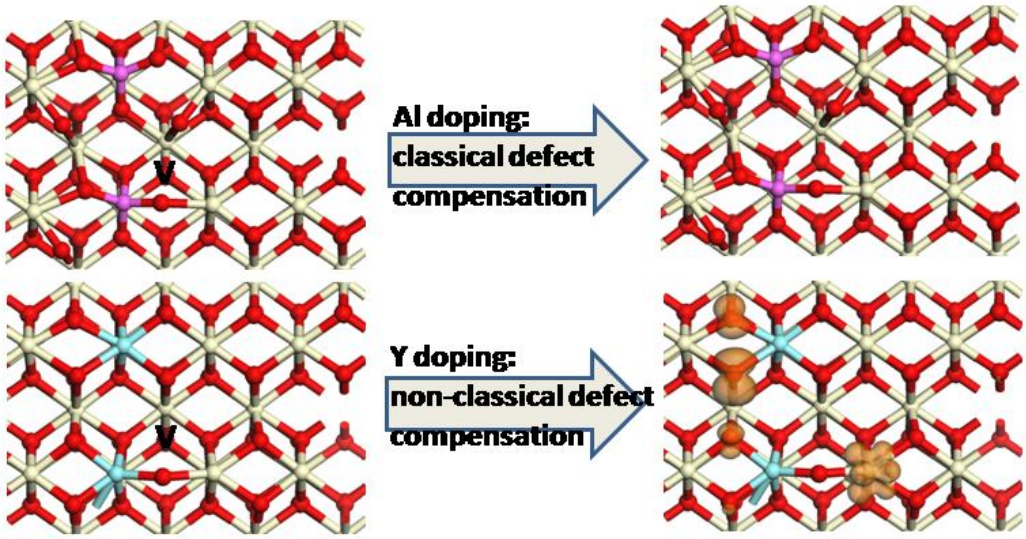
74. Nolan, M. *Phys. Chem. Chem. Phys.* Submitted

75. Shannon, R. D.; Prewitt, C. T. *Acta Crystallogr., Sect. B* **1969,** *25,* 925

76. Orera, V. M.; Merino, R. I.; Chen, Y.; Cases, R. Alonso, P. J. *Phys. Rev. B* **1990,** *42*, 9783

77. Azzoni, C. B.; Paleari, A. *Phys. Rev. B* **1996,** *53,* 5

Table of Contents Graphic



The most stable defect site in the trivalent doped CeO_2 (110) surface depends on the dopant ionic radius